ORAL/POSTER REFERENCE: ICF100575OR

ATOMISTIC SIMULATIONS OF THE MECHANICAL RESPONSE AND MODES OF FAILURE IN METALS AT FINITE STRAIN

J. Zhao[1,2], S. Chantasiriwan[1], D. Maroudas[2], and F. Milstein[1,3]

Departments of [1]Mechanical Engineering, [2]Chemical Engineering, and [3]Materials
University of California, Santa Barbara
Santa Barbara, CA 93106, U.S.A.

ABSTRACT

Isostress molecular dynamics and lattice statics methods have been used to compute theoretical responses of metals to various modes of loading at finite strain, with particular attention to elastic instabilities at points of bifurcation, as well as to post bifurcation phenomena leading to phase change or material failure. The example of nickel in [100] and [110] loading is presented in detail. Interatomic interactions are expressed both by simple Morse pair potentials and by more accurate semi-empirical embedded-atom-method potentials that have been parametrized specifically for studies of crystal elasticity at finite strain. The mechanical responses and failure modes are strongly influenced by crystalline symmetries and incipient bifurcations.

KEYWORDS

Crystals, molecular dynamics, stability, bifurcations, theoretical strength

INTRODUCTION

A number of years ago, Hill [1] observed that "Single crystals free from lattice imperfections are used increasingly as microstructural components. Perfect crystals are capable of elastic strains well beyond what can properly be treated as infinitesimal. Their response to general loading is virtually unknown and is doubtless complex…" In this context, Milstein and Chantasiriwan [2] noted that "Atomistic model computations can shed light on these complexities, particularly when comprehensive comparisons are made among different metals, crystal structures, and loading directions." Topics of current interest [2-4] include theoretical strength, stability, bifurcation, and failure modes at large strain. Here, we employ both the methods of lattice statics (LS), in which stable as well as unstable homogeneous deformation paths are studied, and the isostress molecular dynamics (IMD) ansatz Lagrangian of Parrinello and Rahman (P&R) [5], in which inhomogeneous bifurcations can occur naturally. Extensive series of LS [6a] and IMD [6b] simulations have been carried out; initial results have appeared elsewhere [2,4]. The LS

computations employ an embedded-atom method (EAM) [7] that reproduces identically all second and third order elastic moduli C_{ij} and C_{ijk}, atomic volume V, and cohesive energy E, and yields good theoretical pressure-volume and phonon-dispersion curves, when compared with experiment. The IMD simulations employ Morse interatomic potentials that were fit to two second order elastic moduli and atomic volume [8]; such potentials have been widely used in previous LS computations and yield large strain behavior in excellent qualitative agreement with more rigorous atomic models and experiment [8,9]. In this paper, we examine the behavior of nickel (Ni) under [100] and [110] loading as a particular example.

RESULTS AND DISCUSSION

Figure 1 shows the LS and IMD mechanical responses of the Ni Morse model; the LS behavior is typical of that previously observed for the complete family of Morse function crystals [8-10], as well as for quantum mechanically based pseudopotential models [11]; complete expositions of the LS response have appeared elsewhere [8,11]; a cursory description is provided here. The crystal structure on the primary path (solid line) of Fig. 1a (and throughout Figs. 1b-d) is tetragonal ($l_1 \neq l_2 = l_3$, in general), with uniaxial load l_1 (per unit reference area) applied parallel to the [100] direction; transverse loads $l_2 = l_3 = 0$. Uniaxial stress $s_1 = l_1 / l_2 l_3$, where l_i is the length of a fiber divided by its length in a reference state; the reference state here is the unstressed face centered cubic (fcc) configuration F on the primary path of Fig. 1a. The primary path contains two additional unstressed states, body centered cubic B and a special tetragonal configuration T, and two invariant branch points [8,12], at which the tetragonal crystal

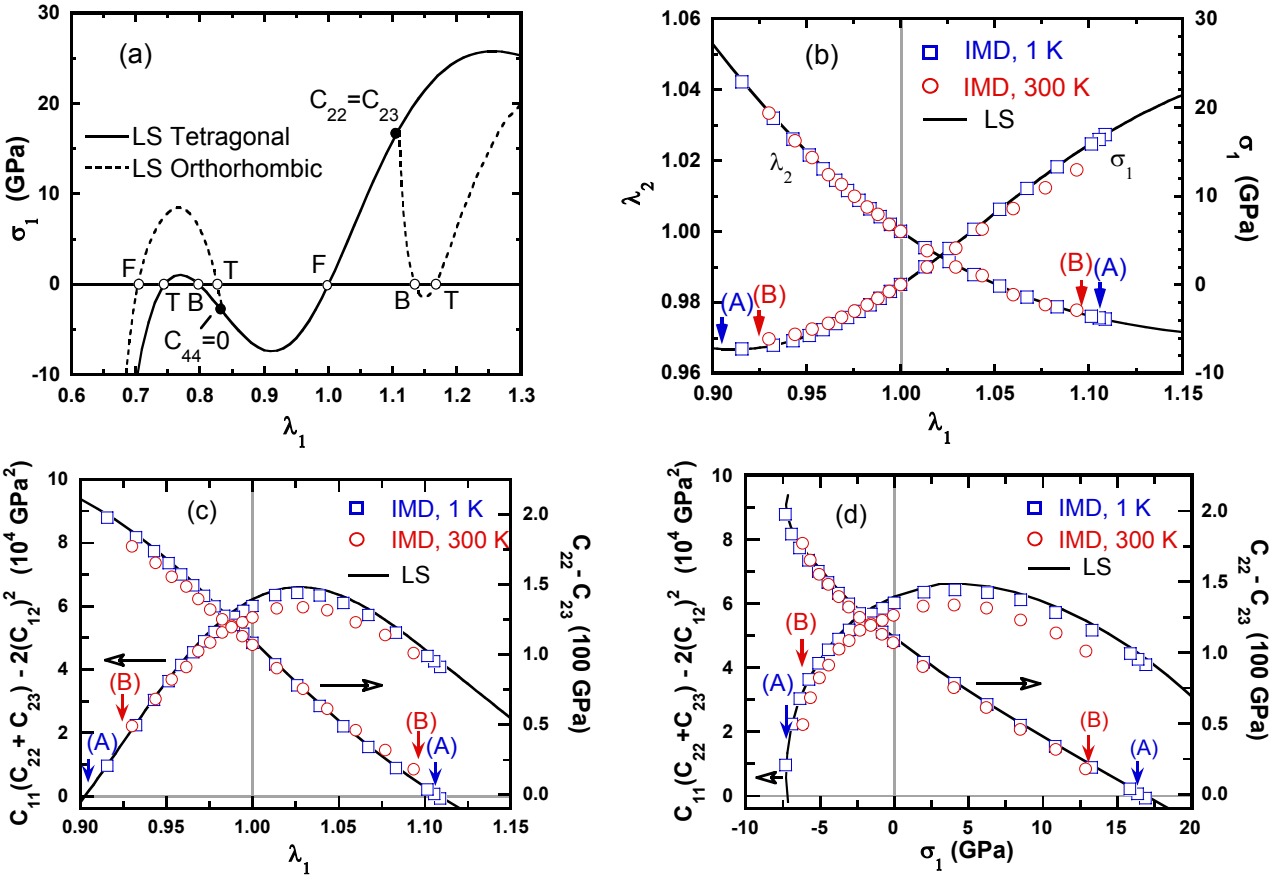

Figure 1: Mechanical response of Morse Ni in (a) [100] and [110] and (b)-(d) [100] loading

can bifurcate homogeneously, under strict uniaxial load, from the primary tetragonal path to a secondary orthorhombic path (dashed lines). Under such branching, second order moduli relations identify the branch points; relations with higher order moduli characterize the branching, as is discussed below, in connection with the EAM results. The primary path may be considered as face centered (fc) or body centered (bc) tetragonal. With the moduli reckoned to the fc axes (as in Figs. 1c,d), the left hand (lh) and right hand (rh) branch points occur respectively, at $C_{44} = 0$ and $C_{22} - C_{23} = 0$; conversely, if the moduli were reckoned to the bc axes, the lh and rh branch points, respectively, would coincide with $C_{22} - C_{23} = 0$ and $C_{44} = 0$ [8,11]. At a "$C_{22} = C_{23}$" eigenstate, to first order, the homogeneous eigendeformation is $dl_1 = 0, dl_2 = - dl_3$, with $dl_1 = dl_2 = dl_3 = 0$, where d indicates incremental change. The crystal thus becomes body centered orthorhombic (bco) on the lh secondary branch and face centered orthorhombic (fco) on the rh branch; the lh and rh secondary paths also contain, respectively, the unstressed F and B structures, although oriented with the load parallel to the [110] directions of *these* cubic structures. Thus, the respective secondary paths also represent primary paths of [110] uniaxial loading of the F and B crystals. The branch paths and symmetries have profound effects on crystal elasticity [8,9,11]; e.g., note the considerably smaller value of the (local) maximum in s_1 in [110] loading than in [100] loading of fcc Ni, owing to the incipient bifurcation at the lh branch point.

We turn next to the topic of stability. In the Morse model of Ni, states T and B are elastically unstable; the stable ranges in Fig. 1a are thus on the tetragonal and the bc orthorhombic paths, in the "neighborhoods" of states F. The use of elastic moduli in assessing stability at finite strain has been discussed elsewhere [1,8,12]; here we simply note that, as criteria for stability on the tetragonal path, "$C_{22} = C_{23}$" locates an invariant eigenstate (its location is independent of the choice of geometric parameters q_r in the definitions $C_{rs} = \partial^2 E / \partial q_r \partial q_s$) [12], while "$D^o \; C_{11}(C_{22} + C_{23}) - 2C_{12}^2 = 0$" occurs where the conjugate variable p_r in the relationship $dp_r = C_{rs}\, dq_s$ is stationary, and thus depends on the choice of q_s [12]. The C_{rs} represented in Figs. 1c,d are the Green moduli; and thus, in these figures, D=0 at the minimum value of the Green conjugate stress, which varies as l_1 / l_1.

Figures 1b-d compare the LS and IMD mechanical responses of Ni under [100] tensile ($l_1 > 1$) and compressive ($l_1 < 1$) loading. In the IMD simulations, the Ni crystal was first equilibrated in a tetragonal configuration at constant temperature T and constant uniaxial [100] stress. Either this equilibrated state remained stable indefinitely, or the crystal subsequently lost stability; both isothermal and adiabatic transformations were studied. The equations of motion in the IMD simulations were integrated using a fifth-order Gear predictor-corrector algorithm [13]. Isothermal conditions were maintained by rescaling the atomic velocities at each time step. The dimensionless fictitious supercell mass W in the P&R Lagrangian was taken to be $W = 20$. The time step size Dt was typically about 10^{-15} s; numerical accuracy and stability were tested for each thermodynamic state examined in our simulations. The initial configuration was an fcc crystal represented by a cubic supercell. For all of the IMD results reported in this paper, the simulation supercell contained 2048 atoms, periodic boundary conditions were employed, and the Morse potential cut-off distance was 5.6294 Å. Systematic convergence tests confirmed that this supercell size does not affect the mechanistic details of the transition under consideration. The C_{rs}, at finite temperature, were computed from canonical fluctuation formulae [14].

States (A) and (B) in Figs. 1b-d indicate where stability was first lost in IMD simulations at 1 and 300 K, respectively. At 1 K, the crystal becomes unstable very near the states $C_{22} = C_{23}$ in tension and $D = 0$ in compression (states (A)). At elevated temperature, the instabilities occur

earlier (states (B)), well before $C_{22} = C_{23}$ and $D = 0$; thus thermal activation "overcomes" the elastic strain energy barrier to bring about transformation.

We concern ourselves next with the tensile instability, which leads to fracture. (The compressive instability, which results in transformation to a hexagonal close packed (hcp) structure in adiabatic simulations, or to faulted hcp in isothermal simulations, will be discussed elsewhere [6b].) Previously, P&R [5] examined the behavior of the Morse Ni model in an adiabatic IMD simulation at and also found failure in the neighborhood of the $C_{22} = C_{23}$ state that was identified earlier by Milstein and Farber [10]. Here, we delve deeper into the failure phenomenon by examining (i) the influence of temperature and stress upon the elastic moduli and points of instability and (ii) the details of atomic movements during isothermal IMD simulations of failure.

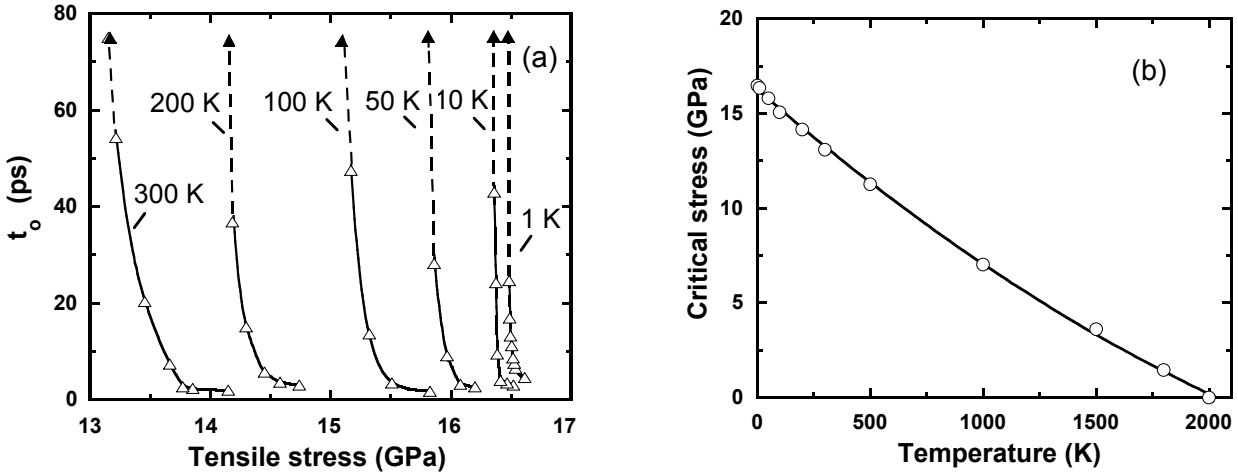

Figure 2: Determination of critical stress and its dependence on temperature

Figure 2a illustrates, for selected values of T, the stress dependence of the time t_o required for the onset of instability adiabatically, with T (of the equilibrated state) as a parameter; the asymptotic limits of stress at which the instabilities are not observed after "infinitely" long times are referred to as the critical stresses s_c. Values of s_c are indicated by solid triangles in Fig. 2a, and a complete set of s_c values is plotted vs T in Fig. 2b; s_c is seen to decrease continuously and monotonically with T, vanishing at the theoretical melting point of about 2000 K.

The mechanism of bifurcation is seen in Figs 3a-j, which show the computer generated evolution of the atomic configurations during an isothermal IMD simulation at 1 K and 17.05 GPa. This stress is slightly greater than the critical stress of 16.5 GPa at 1 K. The load is [100] uniaxial, and thus is perpendicular to the plane of the paper in Figs. 3a-d, and is vertical and parallel to the plane of the paper (i.e. the $(1\bar{1}0)$ plane) in Figs. e-j. At $t = 0$ ps, the crystal is face centered tetragonal, with lattice parameters $a_1 \neq a_2 = a_3$; the predicted bifurcation, $da_2 = -da_3$, $da_1 = 0$, is seen to have initiated in frame b, after about 10 ps. However, the bifurcation does not occur homogeneously throughout the crystal, but occurs in alternating domains that bifurcate with $da_2 > 0$, $da_3 < 0$ and $da_2 < 0$, $da_3 > 0$. In this stage, the atoms remain within their (100) planes, which in themselves remain fairly flat and parallel to each other, as seen in frame f. As the instability proceeds, however, the atoms tend to "shear" out of the (100) planes, which, in turn, leads to void formation and failure. The initial bifurcation is thus a precursor to the ultimate failure. The shearing is seen predominantly in frame h. Supercells containing as many as 16,384 atoms were tested and found to exhibit similar bifurcation and failure responses.

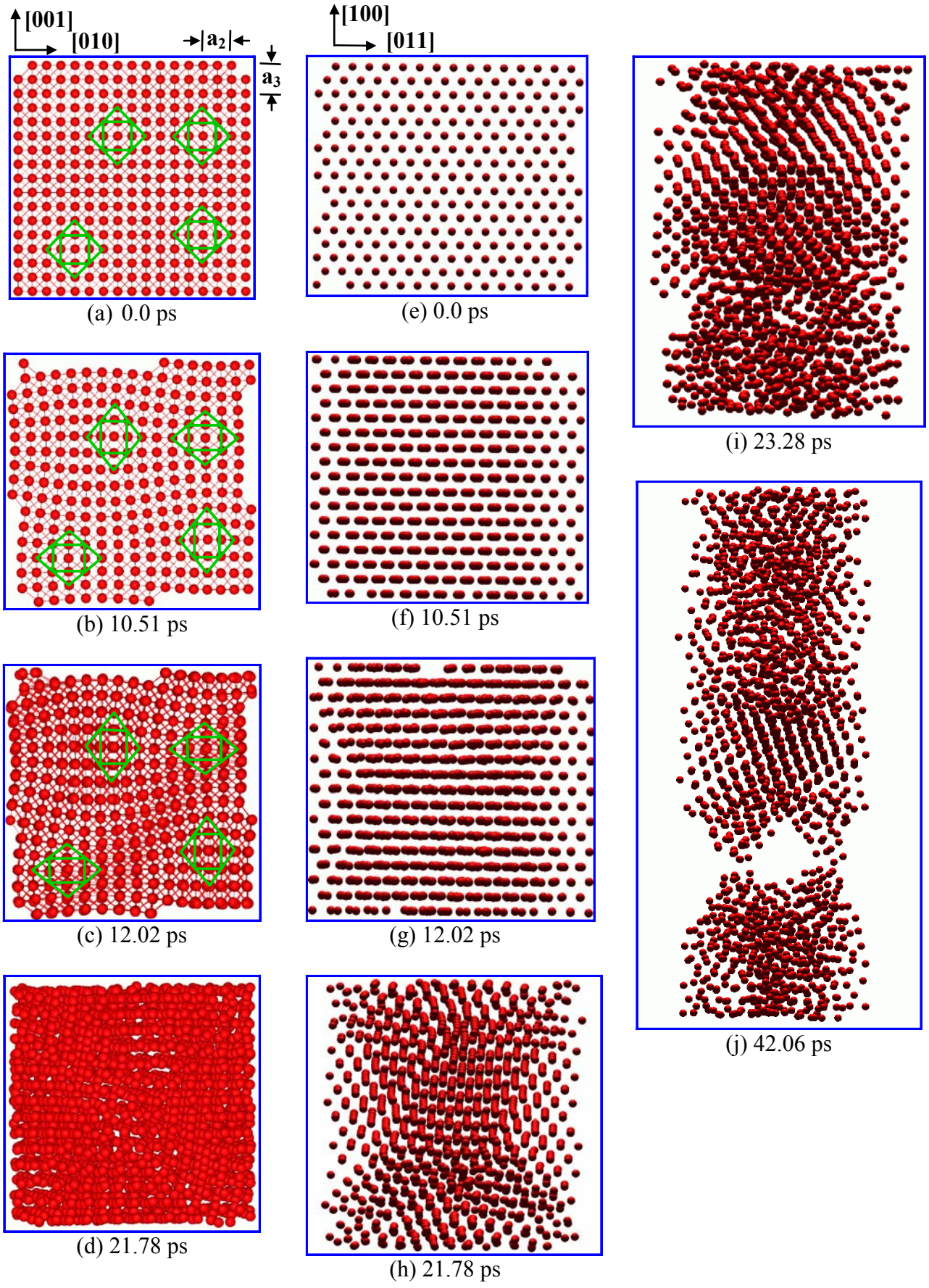

Figure 3: Evolution of atomic configurations during bifurcation and failure in an isothermal IMD simulation of Ni under 17.05 GPa [100] tensile stress at T=1 K

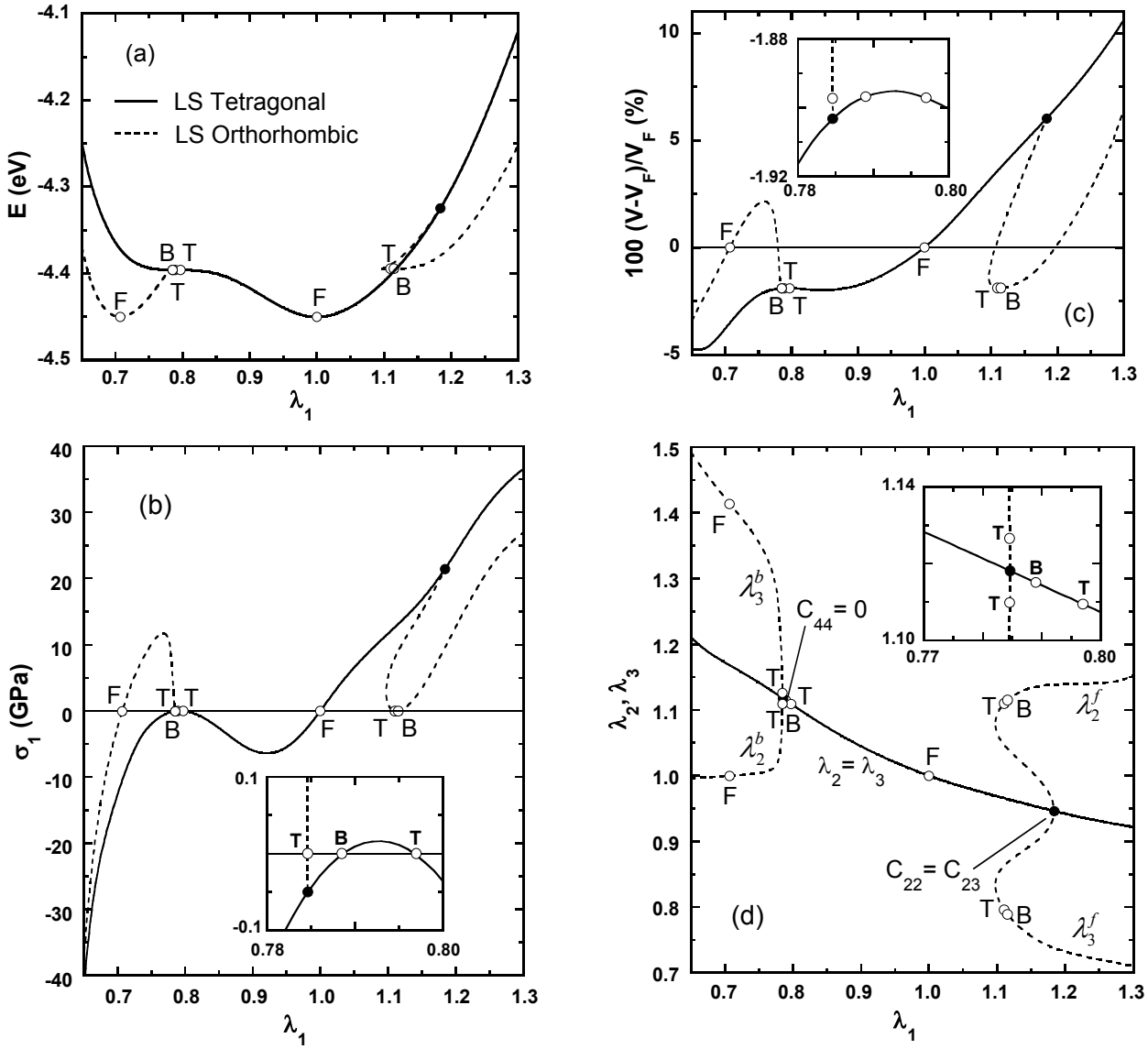

Figure 4: Mechanical response of the EAM model of Ni in [100] and [110] loading

Finally, we examine the LS behavior of the EAM model of Ni, and compare it to that of the Morse model. The EAM model is generally considered as more rigorous in that is has more substantial bases in theory. Also, its linear and non-linear elastic properties in the unstressed fcc state are identically in accord with experiment. As seen from Figs. 4, there is general agreement between the Morse and EAM models, in that both models: (i) exhibit bifurcations at $C_{44} = 0$ and $C_{22} = C_{23}$, leading to orthorhombic structures under uniaxial stress, (ii) contain the unstressed F and T states on the bc orthorhombic (lh) branch, and (iii) have the unstressed B and T configurations on the fc orthorhombic (rh) branch. Also, as in the case of the Morse model, in the EAM model, the crystal structures (and lattice parameters) in the states F, B, and T on the primary path are identical to the corresponding structures in states F, B, and T on the orthorhombic path, but differently oriented with respect to the loading direction; i.e., the loading direction is parallel to the [110] axes of the cubic crystals F and B that reside on the secondary paths.

There is also reasonable quantitative agreement, i.e. s_c is 17 and 21 Mpa, respectively, in the Morse and EAM models at the LS tensile instability (i.e. at $C_{22} = C_{23}$); the respective maximum stresses s_m on the primary path are 26 and 39 MPa, so s_c / s_m is 0.65 in the Morse

model and 0.55 in the EAM model. One noticeable difference, however, is the slope dl_1/dl_1 of the secondary path at the rh branch point, which is positive in the EAM model but negative in the Morse model; such branching, with positive slope, has not heretofore been observed in prior computations. Whether or not the slope of the fco branch path influences the IMD bifurcation response is yet to be determined. The slope on the secondary path at $C_{22} = C_{23}$ is given by [15]

$$\frac{dl_1}{dl_1} = \left\{ c_{11} - \frac{c_{12}^2}{c_{22}} - \left\{ \frac{[2c_{22}(c_{123} - c_{122}) + c_{12}(c_{222} - c_{223})]^2 / c_{22}}{2c_{22}(c_{2222} - 4c_{2223} + 3c_{2233})/3 - (c_{222} - c_{223})^2} \right\} \right\} \qquad (1)$$

where, $c_{ij..} \equiv \partial^2 E / \partial l_i \partial l_{j..}$. The term in brackets [ ] is the slope on the primary path at the branch point, which must be positive if branching terminates stability; thus the expression in the brackets { }, which contains the higher order moduli, must be less than $c_{11} - c_{12}^2/c_{22}$ for positive slope on the secondary path at $c_{22} = c_{23}$. We have used lattice summations to calculate the moduli in both the Morse and EAM models, to fourth order, and verified Eqn. 1 by comparison with the slope dl_1/dl_1, computed directly on the branch path at $c_{22} = c_{23}$.

CONCLUSIONS

Reasonably good agreement is found between the results of Morse model and (more sophisticated) EAM model lattice statics simulations of uniaxial loading of face centered cubic Ni single crystals. For both models, under [100] uniaxial loading, a branch point is found in tension at the invariant "$C_{22} = C_{23}$" eigenstate. The associated homogeneous eigendeformation leads to branching from the tetragonal crystal structure to body centered orthorhombic, via the bifurcation $\delta a_1 = 0$, $\delta a_2 = -\delta a_3$, with the load ℓ_1 remaining uniaxial, i.e., $\delta\ell_1 = \delta\ell_2 = \delta\ell_3 = 0$ (the 1-direction is coincident with the [100] axis, the transverse 2- and 3-directions are [010] and [001]).

In isostress molecular dynamics simulations of [100] loading of Morse model Ni crystals, it is also found that stability in tension is lost as elastic moduli C_{22} and C_{23} approach equality. However, the "predicted bifurcation" occurs locally, rather than uniformly; as shown by the computer generated evolution of the atomic configurations in the isothermal, isostress molecular dynamics simulations, during bifurcation and subsequent fracture. That is, the crystal's lattice parameters bifurcate inhomogeneously, with the $\delta a_1 = 0$ and, in alternating domains, $\delta a_2 = -\delta a_3 > 0$ and $\delta a_2 = -\delta a_3 < 0$. The bifurcation occurs as a precurser to failure. At elevated temperatures, thermal activation causes lattice instability prior to the convergence of C_{22} and C_{23}. The critical stress for failure σ_c is found to decrease continuously and monotonically with temperature, vanishing at the theoretical melting point of about 2000 K.

ACKNOWLEDGMENTS

The Campus Laboratory Collaborations Program of the University of California provided financial support for this work.

S. Chantasiriwan is currently at Thammasat University, Rangsit Campus, Khlong Luang, Pathum Thani 12121

REFERENCES

1. Hill, R. (1975) *Math. Proc. Cambridge Philos. Soc*. 77, 225.
2. Milstein, F. and Chantasiriwan, S. (1998) *Phys. Rev*. B 58, 6006.
3. Morris, J. W. Jr., Krenn, C. R., Roundy, D. and Cohen, M. L. (2000). In*: Phase Transformations and Evolution in Materials*, to be published, Turchi, P.E. and Gonis, A. (Eds). TMS, Warrendale, Pa., 2000.
4. Zhao, J., Maroudas, D. and Milstein, F. (2000) *Phys. Rev*. B 62, 13799.
5. Parrinello, M. and Rahman, A. (1981) *J. Appl. Phys*. 52, 7182.
6. (a) Chantasiriwan, S. and Milstein, F. (b) Zhao, J., Maroudas, D. and Milstein, F., to be published.
7. Chantasiriwan, S. and Milstein, F. (1998) *Phys. Rev.* B 58, 5996.
8. Milstein, F. (1982). In: *Mechanics of Solids,* pp. 417-452, Hopkins, H. G. and Sewell, M. J. (Eds). Pergamon, Oxford.
9. Milstein, F. and Rasky, D. J. (1996) *Phys. Rev*. B 54, 7016; Milstein, F. and Marschall, J. (1988) *Philos. Mag*. A 58, 365.
10. Milstein, F. and Huang, K. (1978) *Phys. Rev*. B 18, 2529; Milstein, F. and Farber, B. (1980) *Phys. Rev. Lett*. 44, 277.
11. Milstein, F. , Marshall, J. and Fang, H. E. (1995) *Phys. Rev. Lett*. 74, 2977.
12. Hill, R. and Milstein, F. (1977) *Phys. Rev*. B 15, 3087.
13. Allen, M. P. and Tildesley, D. J. (1990). *Computer Simulation of Liquids.* Oxford University Press, Oxford.
14. Ray, J. R. (1988) *Comput. Phys. Rep*. 8, 109.
15 Hill, R. (1982) *Math. Proc. Cambridge Philos*. *Soc*. 92, 167.